

On the ‘Loose’ Constraint from IceCube Neutrino Non-Detection of GRB 230307A

XIN-YING SONG ¹

¹*Key Laboratory of Particle Astrophysics, Institute of High Energy Physics, Chinese Academy of Sciences, Beijing 100049, China*

ABSTRACT

The recent extremely bright gamma-ray burst (GRB), GRB 230307A from a binary neutron star merger may offer a good probe for the production of GRB-neutrinos. Within the constraint from IceCube neutrino non-detection, the limits for key physical parameters of this burst are extracted in different scenarios including the fireball, Poynting-flux-dominated (PFD) and hybrid jet. Different from the former nearby ‘monsters’ and due to its smaller isotropic equivalent radiated energy ($E_{\gamma, \text{iso}} \sim 4 \times 10^{52}$ erg), the constraint seems loose if non-thermal neutrinos produced from photomeson interactions are the only consideration. However, a quasi-thermal neutrino emission from hadronuclear processes is constrained in this neutron-rich post-merger environment, and the upper limit of the allowed nucleon loading factor is about a few. Based on this, a discussion is presented on the possible prompt emission mechanism and jet composition for GRB 230307A in the context of multi-messenger astrophysics. **It is worth noting that till now no GRB-neutrinos have been ever detected, even for the two brightest nearby GRBs ever observed (GRB 221009A and GRB 230307A) which have different dissipation mechanisms.**

Keywords: Gamma-ray bursts(629); Neutrino astronomy (1100)

1. INTRODUCTION

For decades, GRBs are proposed to be ultra-high-energy cosmic-ray (UHECR) accelerators and potential sources of astrophysical high energy neutrinos in the GRB fireball scenario (e.g. Paczynski & Xu 1994; Waxman 1995; Vietri 1995; Hümmel et al. 2012). There are mainly two mechanisms for the production of the neutrinos relevant to GRBs: 1) the photomeson ($p\gamma$) process (e.g. Waxman & Bahcall 1997), in which the photons of GRB are guaranteed photons; as predicted in a model-dependent theory, the prompt emission sites are different, which could affect the fluence of this kind of non-thermal (NT) neutrinos (e.g. Zhang & Kumar 2013). 2) Hadronuclear (pn , pp and nn) interactions (e.g. Bahcall & Mészáros 2000; Koers & Giannios 2007; Murase et al. 2013; Bartos et al. 2013) which produce quasi-thermal (QT) neutrinos during the expanding of hot jet material of the outflow; neutrons could be decoupled from protons if the bulk Lorentz Factor (Γ) is large enough. Thus inelastic collisions could occur and

pions could be produced. The neutrinos with 5-10 GeV could be generated after pions decays; alternatively, if the coasting occurs earlier than np decoupling, the dissipation of neutrons via internal collisions between the compound flows may happen, which could also generate QT neutrinos in the sub-TeV range (e.g. Murase et al. 2013). Note that the neutrino emission could occur during the prompt phase of GRB as well as the (choked) jet’s propagation within the macronova/kilonova ejecta or a massive progenitor envelope (e.g. Mészáros & Waxman 2001; Murase & Ioka 2013; Senno et al. 2016; Kimura et al. 2018), as a precursor for GRBs. However, till now, no evident correlation between neutrino events and observed GRBs is observed (e.g. Aartsen et al. 2017; Abbasi et al. 2023a).

It is usually proposed that long GRBs are from the collapses of massive stars, while short GRBs are produced from mergers of compact stars. However, there are some exceptions, such as GRB 060614 (e.g. Gehrels et al. 2006) and GRB 211211A (e.g. Yang et al. 2022). Recently, another exception, GRB 230307A, associated with kilonova emission (Levan et al. 2023b; Fermi GBM Team 2023; Xiong et al. 2023; Svinikin et al. 2023) arises. The isotropic-equivalent radiated energy $E_{\gamma, \text{iso}} \sim 4 \times 10^{52}$ erg of GRB 230307A is smaller compared with other

nearby bright GRBs (e.g., $E_{\gamma,\text{iso}} \sim 10^{54}$ erg for GRB 130427A and $E_{\gamma,\text{iso}} \sim 2 \times 10^{54}$ erg for GRB 221009A), thus it could be inferred that the features of the burst can not be well constrained if the neutrino emission from $p\gamma$ interactions is the only consideration. However, with the favoured redshift $z \sim 0.065$ (e.g. O'Connor et al. 2023; Levan et al. 2023a), d_L^2 of GRB 230307A is about 6 times smaller than that of GRB 221009A, and 37 times smaller than that of GRB 130427A, where d_L is the distance of the GRB source. Therefore it may be still a good probe for the GRB-neutrinos.

It is worth to note that the IceCube Neutrino Observatory provides an upper limit (U.L.) of muon neutrinos (ν_μ), 1.0 GeV cm^{-2} at 90% C.L. (IceCube Collaboration 2023), which seems less constraining compared with $3.9 \times 10^{-2} \text{ GeV cm}^{-2}$ at 90% CL of GRB 221009A (IceCube Collaboration 2022). Besides, there exists a significant photospheric emission in the prompt phase in GRB 230307A, which is different from synchrotron radiation-dominated GRB 221009A whose jet is dominated by the Poynting flux (Yang et al. 2023). The emission mechanism as well as the jet composition could affect the production of the neutrinos (Hümmer et al. 2012; Gao et al. 2012; Pitik et al. 2021), thus one may wonder the limits on key features of this burst within this ‘loose’ constraint in different scenarios of emission mechanism and the jet composition. **The neutrinos annihilation mechanism and magnetohydrodynamic processes both may affect the jet composition, which could occur in the scenarios of massive stars collapse (a single progenitor or binary progenitors, e.g. in a binary-driven hypernova model in Aimuratov et al. (2023)) and mergers of compact stars.**

The paper is organized as follows: in Section 2, the limits for key physical parameters of GRB 230307A are extracted within the constraint of the neutrino fluence in different GRB-neutrino scenarios; in Section 3, basic properties of the prompt emission for GRB 230307A are introduced and discussed; the discussion and summary are given in Section 4.

2. THE POSSIBLE NEUTRINO EMISSIONS FROM GRB 230307A

In this section, we consider the possible neutrino emissions via hadronuclear processes as well as $p\gamma$ interactions. For convenience, we use spectral parameters of GRB 230307A in $[2.2, 11.7]$ s after the trigger time: $\alpha = -0.8$, $\beta = -8$ and $E_{\text{peak}} = 1.1 \text{ MeV}$. The duration is taken to be 40 s and $E_{\gamma,\text{iso}} = 4 \times 10^{52}$ erg. For comparison, GRB 221009A is also analyzed, with parameters of $\alpha = -1.0$, $\beta = -2.3$, $E_{\text{peak}} = 1.0 \text{ MeV}$, a duration time

of 327 s and $E_{\gamma,\text{iso}} = 2 \times 10^{54}$ erg. The convention $Q = 10^n Q_n$ is adopted for CGS units hereafter.

2.1. photomeson ($p\gamma$) process

The decay chains of photomeson interactions for single-pion production are

$$p + \gamma \rightarrow p + \pi^0, \quad (1)$$

$$\pi^0 \rightarrow \gamma + \gamma, \quad (2)$$

and

$$p + \gamma \rightarrow n + \pi^+, \quad (3)$$

$$\pi^+ \rightarrow \mu^+ + \nu_\mu, \quad (4)$$

$$\mu^+ \rightarrow e^+ + \nu_e + \bar{\nu}_\mu. \quad (5)$$

In the processes shown in (3)-(5), one pion could produce four leptons. Before deducing formulae, some important definitions are introduced as below:

- the fractions of energy dissipated in protons, random magnetic fields (with a strength B), and radiated as γ -rays are ϵ_p , ϵ_B and ϵ_γ . The proton energy is estimated via $E_{\text{proton}} = \epsilon_p/\epsilon_e E_{\gamma,\text{iso}}$, with the CR loading factor $\xi_{\text{CR}} = \epsilon_p/\epsilon_e$; note that the mark (') in the superscript denotes that the quantity is in the comoving frame, while an overline denotes the rest frame of proton, hereafter; one has $B' = \left[\frac{L_{\text{tot}}(\epsilon_B/\epsilon_e)}{2R_d^2\Gamma^2c} \right]^{1/2}$ in the comoving frame, where L_{tot} (or E_{tot}) is the total luminosity (or energy);
- the energy distribution of accelerated protons by random magnetic fields is $\frac{dN_p}{dE_p} \propto E_p^{-p}$, where the index $p = 2$ is assumed; $E_{p,\text{max}}$ and $E_{p,\text{min}}$ represent the maximum and minimum energies of accelerated protons in the observer's rest frame; $\frac{dN_p}{dE_p} = \frac{(\epsilon_p/\epsilon_e)E_{\text{tot}}}{\ln(E_{p,\text{max}}/E_{p,\text{min}})} E_p^{-p}$, where $E_{\text{proton}} = \epsilon_p E_{\text{tot}}$; the minimum energy of proton is set to be $E_{p,\text{min}} = \Gamma m_p c^2$ assuming it is rest in the comoving frame; the maximum energy $E_{p,\text{max}}$ is the energy of protons which are accelerated by the magnetic field, and estimated by equating the dynamical timescale $t'_{\text{dyn}} \sim R/\Gamma c$ with the accelerating timescale of protons $t'_{\text{acc}} \sim E'_p/(eB'c)$;
- R_d is the dissipation radius: for photospheric (PH) emissions, $R_{d,\text{PH}} \sim 10^{11}$ cm; for IS mechanism, $R_{d,\text{IS}} \sim 10^{12-13}$ cm; for ICMART mechanism, $R_{d,\text{ICMART}} \sim 10^{15}$ cm; they could be estimated from the parameters of the burst;
- the cross section of $p\gamma$ interaction is $\sigma_{p\gamma} = 5 \times 10^{-28} \text{ cm}^{-2}$; π^+ decay time scales is $\tau_{\pi^+} = 2.8 \times$

10^{-8} s; in the comoving frame, the Lorentz factor of π^+ is denoted as γ'_{π^+} . ε_γ denotes the specific energy of a photon; γ_p , β_p is the Lorentz Factor and velocity of a specific proton in the comoving spectrum, and so on;

- the width of the Breit-Weigner form of $\Delta(1232)$ resonance is $\Delta\bar{\varepsilon}_{\text{pk}} \sim 0.2$ GeV; $\bar{\varepsilon}_{\text{pk}} \simeq 0.3$ GeV are the photon energy at the resonance peak in the photomeson process.

The pion production rate is deduced to calculate the neutrino spectrum¹. $\sigma_{p\gamma}$ is given as a function of the photon energy in the proton-rest frame, $\bar{\varepsilon}_\gamma = \gamma'_p \varepsilon_\gamma (1 - \beta'_p \mu)$, where $\gamma'_p = \varepsilon'_p / (m_p c^2)$, β'_p , ε'_p , $\mu = \cos \theta_p$ are the Lorentz factor of protons, the proton velocity, the photon energy, and the angle between the directions of interacting proton and photon in the comoving frame, respectively. The energy loss rate of protons by pions production is written as

$$t_{p\gamma}^{-1} = c \int d\Omega \int d\varepsilon'_\gamma (1 - \beta'_p \mu) n_\gamma(\varepsilon'_\gamma, \Omega) \sigma_{p\gamma}(\bar{\varepsilon}_\gamma) \kappa_{p\gamma}(\bar{\varepsilon}_\gamma), \quad (6)$$

where $n_\gamma(\varepsilon'_\gamma, \Omega) = dN / (d\varepsilon'_\gamma dV d\Omega)$ and $\kappa_{p\gamma}$ is the inelasticity of the $p\gamma$ interactions. This rate is approximately equivalent to the pion production rate. Then, to convert the integration variable from μ to $\bar{\varepsilon}_\gamma$, the photomeson production rate is represented as

$$t_{p\gamma}^{-1} = \frac{c}{2\gamma_p'^2} \int_{\varepsilon_{\text{th}}}^{\infty} d\bar{\varepsilon}_\gamma \sigma_{p\gamma} \kappa_{p\gamma} \bar{\varepsilon}_\gamma \int_{\bar{\varepsilon}_\gamma / (2\gamma_p')}^{\infty} \frac{d\varepsilon'_\gamma}{\varepsilon_p'^2} n_{\varepsilon'_\gamma}, \quad (7)$$

where we use $n_\gamma(\varepsilon'_\gamma, \Omega) = n_{\varepsilon'_\gamma} / (4\pi)$, $n_{\varepsilon'_\gamma} = dN / (d\varepsilon'_\gamma dV)$, $\beta'_p \sim 1$. Note that the energy threshold ε_{th} is determined by the Breit-Weigner mass and width of $\Delta(1232)$ resonance. We have

$$\sigma_{p\gamma} \kappa_{p\gamma} \approx \sigma_{\text{pk}} \kappa_{\text{pk}} \Delta \bar{\varepsilon}_{\text{pk}} \delta(\bar{\varepsilon}_\gamma - \bar{\varepsilon}_{\text{pk}}). \quad (8)$$

The pion production efficiency, or the fraction of CR protons producing pions is given by $f_{p\gamma} = \min(1, t_{p\gamma}^{-1} / t_{\text{dyn}}^{-1})$. The distribution of the target photons in the form of

$$n_\gamma(\varepsilon_\gamma) = \frac{dN_\gamma(\varepsilon_\gamma)}{d\varepsilon_\gamma} = n_{\gamma,b} \begin{cases} \varepsilon_{\gamma,b}^{-\alpha} \varepsilon_\gamma^\alpha, & \varepsilon_\gamma < \varepsilon_{\gamma,b} \\ \varepsilon_{\gamma,b}^{-\beta} \varepsilon_\gamma^\beta, & \varepsilon_\gamma \geq \varepsilon_{\gamma,b} \end{cases} \quad (9)$$

where $\varepsilon_{\gamma,b} = \frac{(\alpha-\beta)E_{\text{peak}}}{\alpha+2}$ and $n_{\gamma,b}$ is the specific photon number of $\varepsilon_\gamma = \varepsilon_{\gamma,b}$. About half of the $p\gamma$ inelastic

interactions produce charged pions with the energy of $\varepsilon_\pi \approx 0.2\varepsilon_p$. The high-energy pions lose their energies by either synchrotron radiation or dynamical expansion before they decay to neutrinos. Considering the average energy fraction in pion decaying to four leptons, $\varepsilon_\nu = 1/4\varepsilon_\pi$ and half decays to charged pions in $p\gamma$ inelastic interaction, the differential total muon neutrino energy is

$$E_\nu^2 N_{E_\nu} \approx \frac{1}{8} f_{p\gamma} f_{\pi,\text{sup}} E_p^2 N_{E_p}, \quad (10)$$

where $f_{\pi,\text{sup}}$ is the pion cooling suppression factor, and approximated to be

$$f_{\pi,\text{sup}} \approx 1 - \exp\left(-\frac{t'_{\pi,\text{cl}}}{t'_{\pi,\text{dec}}}\right), \quad (11)$$

where $t'_{\pi,\text{cl}} = 6\pi m_\pi^4 c^3 / (m_e^2 \sigma_T B'^2 \varepsilon'_\pi)$ is the pion cooling time, and $t'_{\pi,\text{dec}} = \varepsilon'_\pi \tau_\pi / (m_\pi c^2)$ is the decay time of charged pions. If $\varepsilon'_\pi < \varepsilon'_{\pi,\text{cooling}}$ ($\varepsilon'_{\pi,\text{cooling}} = \frac{\Gamma}{1+z} \sqrt{\frac{6\pi m_\pi^5 c^5}{m_e^2 \sigma_T \tau_\pi B'^2}}$ is the critical cooling energy estimated by equating $t'_{\pi,\text{syn}}$ and $t'_{\pi,\text{dec}}$), the cooling effect is not efficient, and $f_{\pi,\text{sup}} \approx 1$, while $f_{\pi,\text{sup}} \approx (\varepsilon'_\pi / \varepsilon'_{\pi,\text{cooling}})^2$ for $\varepsilon'_\pi > \varepsilon'_{\pi,\text{cooling}}$.

Considering the cooling process which causes the second break in neutrino spectrum² and Equations (7)–(10), the neutrino spectrum could be described as a power law with two breaks,

$$n_\nu(E_\nu) = \frac{dN_\nu(E_\nu)}{dE_\nu} = n_{\nu,1} \begin{cases} \varepsilon_{\nu,1}^{\alpha_\nu} E_\nu^{-\alpha_\nu}, & E_\nu < \varepsilon_{\nu,1} \\ \varepsilon_{\nu,1}^{\beta_\nu} E_\nu^{-\beta_\nu}, & \varepsilon_{\nu,1} \leq E_\nu < \varepsilon_{\nu,2} \\ \varepsilon_{\nu,1}^{\beta_\nu} \varepsilon_{\nu,2}^{\gamma_\nu - \beta_\nu} E_\nu^{-\gamma_\nu}, & E_\nu \geq \varepsilon_{\nu,2} \end{cases} \quad (12)$$

and one has

$$\alpha_\nu = p + 1 + \beta, \quad \beta_\nu = p + 1 + \alpha, \quad \gamma_\nu = \beta_\nu + 2. \quad (13)$$

$\varepsilon_{\nu,1}$ could be derived in two different cases according to $\tau_{p\gamma}$. If $\tau_{p\gamma} < 5$, one has

$$\varepsilon_{\nu,1} = \varepsilon_{\nu,1}^0 = 6.33 \times 10^5 \text{ GeV} (1+z)^{-2} (\Gamma/300)^2 \left(\frac{\varepsilon_{\gamma,b}}{1 \text{ MeV}}\right)^{-1}. \quad (14)$$

if $\tau_{p\gamma}$ increases above 5, $f_{p\gamma}$ exceeds 0.5 and quickly approaches 1, and the neutrino flux no longer significantly increases with $\tau_{p\gamma}$, and $\varepsilon_{\nu,1}$ has a form of

$$\varepsilon_{\nu,1} = \varepsilon_{\nu,1}^0 \times \left(\frac{\tau_{p\gamma}^{\text{peak}}}{3}\right)^{1+\beta}, \quad (15)$$

¹ The followed deduction could be found in many works (e.g. Kimura 2022) and references therein.

² The second break is caused by $E_{p,\text{max}}$ if the pion cooling is not significant.

where $\tau_{p\gamma}^{\text{peak}}$ is the peak $p\gamma$ optical depth (the one for protons with energy E_p^{peak} to interact with the photons with a peak energy) and described as

$$\tau_{p\gamma}^{\text{peak}} = 8.9 L_{\text{GRB},52} \left(\frac{\Gamma}{300} \right)^{-2} R_{13}^{-1} \left(\frac{\epsilon_{\gamma,b}}{\text{MeV}} \right)^{-1}. \quad (16)$$

$f_{p\gamma \rightarrow N\pi}$ is the fraction of proton energy going into the π production, and one has $f_{p\gamma \rightarrow N\pi} = 1 - (1 - \langle \chi_{p \rightarrow \pi} \rangle)^{\tau_{p\gamma}}$, where $\langle \chi_{p \rightarrow \pi} \rangle = 0.2$ is the the average fraction of energy transferred from protons to pions³.

From Equation (14) and (15), $\varepsilon_{\nu,1}$ is denoted with

$$\varepsilon_{\nu,1} = \varepsilon_{\nu,1}^0 \times \min \left\{ 1, \left(\frac{\tau_{p\gamma}^{\text{peak}}}{5} \right)^{1+\beta} \right\}. \quad (17)$$

$\varepsilon_{\nu,2}$ is relevant to the $\varepsilon'_{\pi,\text{cooling}}$ as

$$\varepsilon_{\nu,2} = \frac{1}{4} D \varepsilon'_{\pi,\text{cooling}}, \quad (18)$$

where D is the Doppler factor and $D \simeq 2\Gamma$ if the observation is head on. The amplitude $n_{\nu,1}$ could be derived from integration of $E_p \frac{dN_p}{dE_p} dE_p$ from $E_{p,\text{min}}$ to $E_{p,\text{max}}$ as

$$n_{\nu,1} = \frac{1}{8} f_p f_{p\gamma \rightarrow N\pi} \frac{\epsilon_p / \epsilon_e E_{\gamma,\text{iso}}}{\ln(\varepsilon_{\nu,2} / \varepsilon_{\nu,1})} \varepsilon_{\nu,1}^{-2}, \quad (19)$$

where $f_p = \frac{\ln(\varepsilon_{\nu,2} / \varepsilon_{\nu,1})}{\ln(E_{p,\text{max}} / E_{p,\text{min}})}$. The observed fluence of the muon neutrinos is

$$E_\nu^2 \phi_\nu(E_\nu) = \frac{E_\nu^2 n_\nu(E_\nu)}{4\pi d_L^2}. \quad (20)$$

With $\Gamma = 400$, $\xi_{\text{CR}} = \epsilon_p / \epsilon_\gamma = 3$ and $\epsilon_B = \epsilon_\gamma$ for each emission mechanism, the predicted neutrino spectra from GRB 230307A and 221009A are shown in Figure 1 (a) and (b). The fluence level of GRB 230307A with assuming a photospheric emission is the maximum of three mechanisms, which is about two orders of magnitude smaller than the U.L. of 1 GeV cm^{-2} , and one order of magnitude smaller than that of GRB 221009A. Furthermore, as shown in Figure 1 (c) and (d), ξ_{CR} of the excluded region is extremely large (even if with a small $R_d = 10^{11} \text{ cm}$ in Figure 1 (c)), which seems unreasonable for GRBs. The case is similar and the ξ_N is still large (> 10) if with an U.L. of one order of magnitude lower (0.1 GeV cm^{-2}). Thus, the emission mechanisms as well as ξ_{CR} are not constrained within the U.L. of the neutrino production via $p\gamma$ interactions.

³ $\tau_{p\gamma} = 3$ is used in Zhang & Kumar (2013), and $f_{p\gamma \rightarrow N\pi}$ is much nearer to 100% with $\tau_{p\gamma} = 5$ shown in Ai & Gao (2023).

2.2. hadronuclear process

2.2.1. neutron-proton (np) decoupling

In the neutron-rich environment, an admixture of baryons exist in the outflow besides of photons and e^\pm . During the expanding of the outflow, the electrons can exchange energy with photons via Compton scattering and with protons via Coulomb collisions; however, for the neutrons, only protons have enough mass to collider with them and cause a collisional np coupling (e.g. Rossi et al. 2006). This means that, if the neutron-to-proton ratio (denoted as ζ_n) is large so that there are not enough protons, or Γ is large enough (above the the critical value Γ_{np}), the neutrons can not be accelerated so fast along with the other outflow component, even if they have drifted into the outflow in the early stage of acceleration. In this scenario the np decoupling happens. After decoupling both n and p continue to coast together due to inertia, and their relative velocities could reach the threshold for inelastic collisions, of which decay chains are

$$p + n \rightarrow p + n + \pi^0, \quad (21)$$

$$p + n \rightarrow n + n + \pi^+, \quad (22)$$

$$p + n \rightarrow p + p + \pi^-. \quad (23)$$

The charged pions and their secondary particles muons, could produce leptons via the same decay chains as those in processes (4)-(5). The detected fluence of muon neutrinos number from np decoupling could be described as,

$$\Phi_{N_{\nu_\mu}} = \frac{N_n N_{\nu_\mu} \tau_{np}}{4\pi d_L^2}, \quad (24)$$

where N_n denotes the number of neutrons contained in the outflow, N_{ν_μ} denotes the number of muon neutrinos created per inelastic np interaction with considering the neutrinos flavour mixing, and τ_{np} denotes the optical depth for the np collision, which could be approximated to the inelastic np interaction probability.

In the acceleration phase, the radius (R) and $\Gamma(R)$ has a relation of

$$\Gamma(R) = \Gamma_0 \left(\frac{R}{r_0} \right)^m, \quad (25)$$

where r_0 is the initial radius of acceleration and Γ_0 is the initial Lorentz factor. r_0 is taken to be 10^8 cm ⁴; m ranges from $1/3$ to 1 . For the rapid acceleration of the fireball, $m = 1$, while for the slow acceleration by the Poynting flux, m could be $1/3$. Note that in a collapsar

⁴ $r_0 = 10^8 \text{ cm}$ is the mean value of the initial acceleration radius (Pe'er et al. 2015).

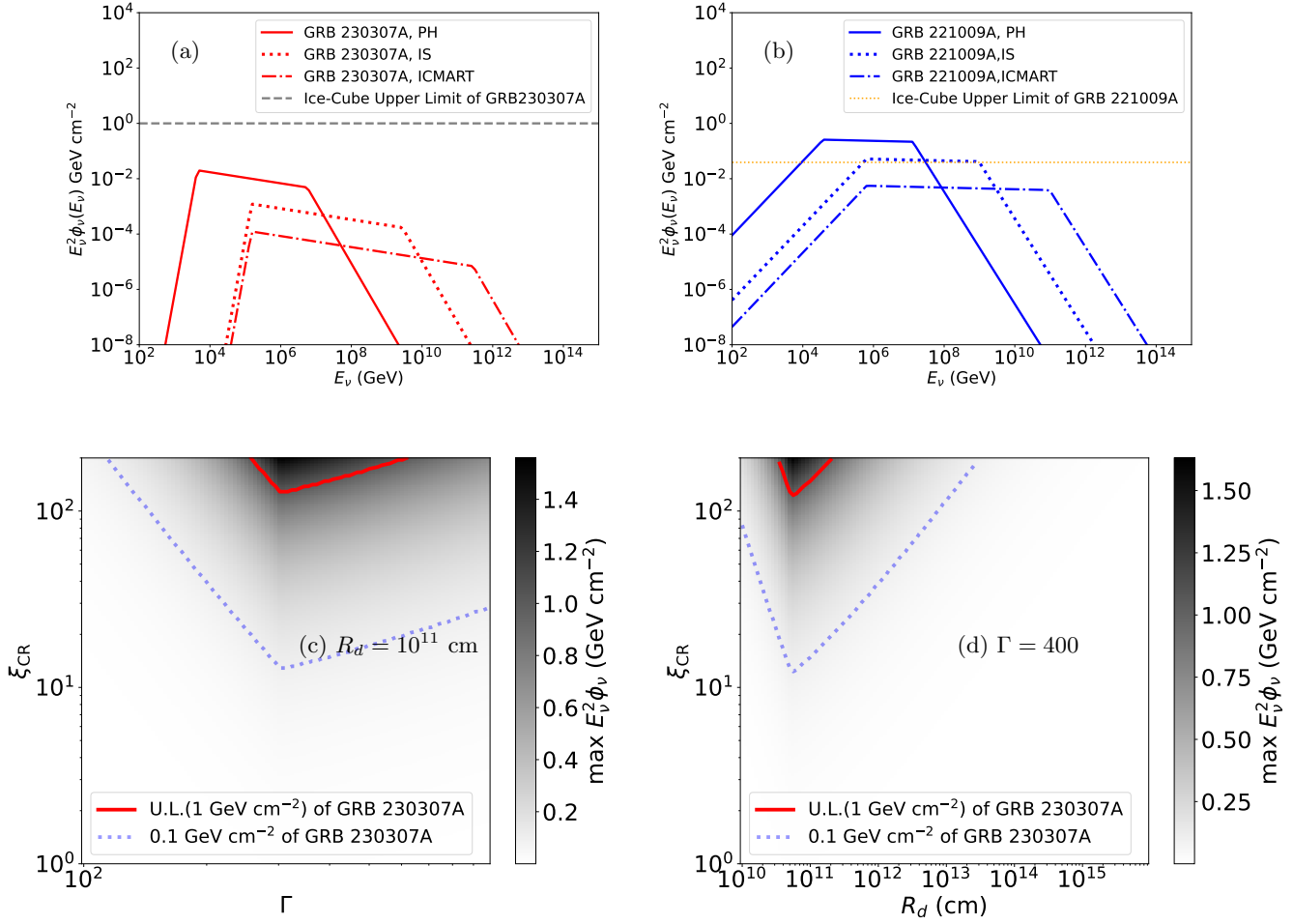


Figure 1. (a) and (b) the non-thermal neutrino spectra with $\Gamma = 400$ for GRB 230307A and GRB 221009A of different emission mechanisms. For GRB 221009A, f_p is calculated to be about 0.3, 0.5 and 0.3 for PH, ICMART and IS models respectively; for GRB 230307A, f_p is calculated to be about 0.3, 0.7 and 0.5 for PH, ICMART and IS models respectively. (c) and (d) are allowed ranges of Γ , R_d and ξ_{CR} . The solid red line denotes the U.L. at 90% C.L. of GRB 230307A. The blue dotted line denotes one order of magnitude lower than U.L. = 1 GeV cm^{-2} . The allowed ranges are below the corresponding lines, while the excluded ranges are above them, the same below.

scenario of a massive star, $2/3 < \zeta_n \simeq 1$, while in a NS-NS merger scenario, $\zeta_n \geq 1$ (e.g. Bahcall & Mészáros 2000). In the neutron-rich environment after the NS-NS merger for GRB 230307A, the electron (or proton) to nucleon ratio $Y_e = \frac{1}{1+\zeta_n} \sim 0.15$ for a fast dynamical ejecta and 0.3 for slow disk-wind ejecta as reported in Bulla et al. (2023), which corresponds to $2.3 < \zeta_n < 5.7$. The neutrons could penetrate the outflow, and be contained in the outflow (e.g. Beloborodov 2003).

First, the fireball scenario is considered with $m = 1$. The np collision time scale is $t'_{np} \approx 1/(n'_p \sigma_{np} c)$, where the $\sigma_{np} \approx 3 \times 10^{-26} \text{ cm}^2$ is the approximate np cross section, $n'_p \approx L_p/(4\pi R^2 \Gamma \eta m_p c^3)$ is the proton density, L_p is the luminosity of the proton outflow and η is the maximum Lorentz Factor that all the energy is used to accelerate the protons. By equat-

ing t'_{np} and the dynamical time scale $t'_{\text{dyn}} \approx R/(\Gamma c)$, the decoupling radius is estimated to be $r_{\text{dec}} \approx 8.7 \times 10^{11} \text{ cm } L_{p,53}^{1/3} r_{0,11}^{2/3} \Gamma_{0,1}^{-2/3} \eta_{2.9}^{-1/3}$, at which the Lorentz factor becomes (Bahcall & Mészáros 2000; Murase et al. 2022),

$$\Gamma_{n,\text{dec}}^0 \approx 65 L_{p,53}^{1/3} r_{0,11}^{-1/3} \Gamma_{0,1}^{1/3} \eta_{2.9}^{-1/3}. \quad (26)$$

Note that Γ must be greater than Γ_{np} which is

$$\Gamma_{np} \approx \left(\frac{\sigma_{np} L_p \Gamma_0}{4\pi m_p c^3 r_0} \right)^{1/4} = 477 L_{p,53}^{1/4} \Gamma_0^{1/4} r_{0,8}^{1/4}. \quad (27)$$

Thus the Lorentz Factor of neutron at the decoupling time is

$$\Gamma_{n,\text{dec}} = \min(\Gamma_{n,\text{dec}}^0, \Gamma_{np}) \quad (28)$$

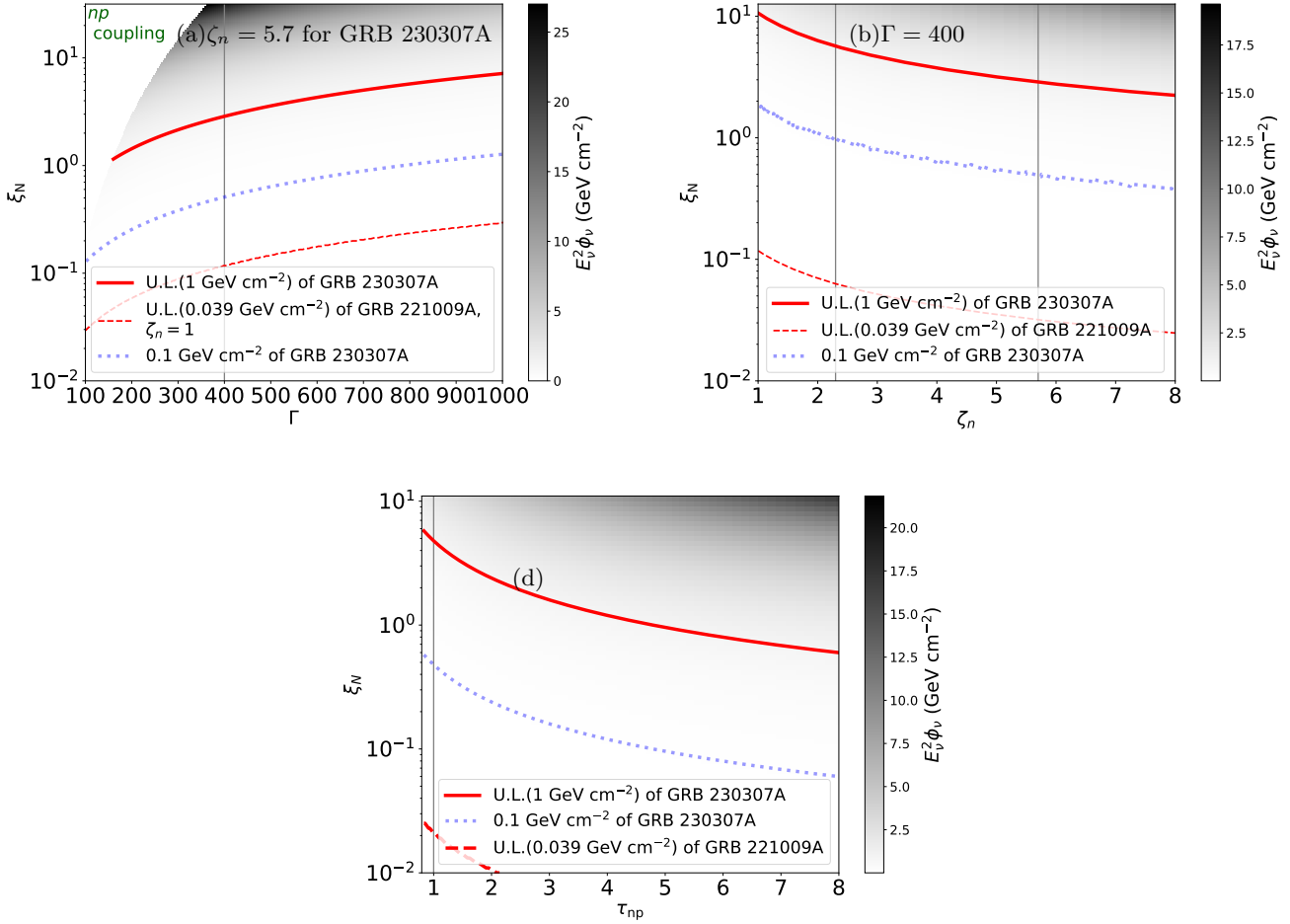


Figure 2. (a), (b) are allowed and excluded ranges of Γ , ξ_N and ζ_n in np decoupling mechanism. The blank around lower Γ and higher ξ_N is the np coupling region where $\Gamma < \Gamma_{np}$. The red dashed line denotes that of GRB 221009A. The gray vertical lines denote the $\Gamma = 400$ for (a) and $\zeta_n = 2.3$ and 5.7 for (b). (c) The allowed and excluded ranges of ξ_N in the np collision mechanism. The vertical line denotes $\tau_{np} = 1$.

decoupling radius by definition, and the energy of QT neutrinos is

$$E_{\nu}^{\text{QT}} \approx 0.1 \Gamma_{n,\text{dec}} m_p c^2 / (1+z), \quad (29)$$

which predicts $\sim 1 - 10$ GeV neutrinos with $m_p c^2 = 0.938$ GeV and $\Gamma_{n,\text{dec}}$ is mild ($\lesssim 100$). The neutrino energy fluence is estimated to be

$$E_{\nu}^2 \phi_{\nu} \approx \frac{1}{12} \frac{(1+z)}{4\pi d_L^2} \zeta_n \left(\frac{\Gamma_{n,\text{dec}}}{\Gamma} \right) E_{\text{proton}}, \quad (30)$$

where $\phi_{\nu} = \frac{1}{4\pi d_L^2} \frac{dN_{\nu\mu}}{dE_{\nu\mu}}$. $E_{\text{proton}} \approx \xi_N E_{\gamma}^{\text{iso}}$ is the kinetic energy of the proton outflow and ξ_N is the proton or nucleon loading factor. The coefficient $1/12$ comes from the product of inelasticity (0.5), the fraction of charged pions (2/3) and the energy fraction of ν_{μ} after the flavour mixing (1/4).

Figure 2 (a) and (b) shows the allowed ranges of ξ_N , Γ and ζ_n within the constraint from U.L. of neutrino fluence. With $\Gamma = 400$ and $\zeta_n = 5.7$, the U.L. of ξ_N could reach up to 3. From Figure 2 (b), the U.L. of ξ_N decreases with the ζ_n . With one order of magnitude lower than 1 GeV cm^{-2} , the U.L. of $\xi_N \lesssim 1$ as shown in dotted lines in Figure 2 (a) and (b). Compared with the largest allowed $\xi_N \lesssim 0.1$ for GRB 221009A (with $\zeta_n = 1$), it seems that a heavier baryon loading could be allowed for GRB 230307A.

If another case that the Poynting flux is dominated ($\sigma_0 > 10$, where σ_0 is the Poynting-to-kinetic flux ratio) is considered, the neutrino fluence could be smaller. This is because τ_{np} in Equation (24) has a form of

$$\tau_{np}(m) = \int_{\chi_{\pi}}^{\infty} \left(1 - \frac{0.75}{\ln \chi}\right) (\chi^{-1} - \chi^{-3}) \chi^{-1/m}, \quad (31)$$

where χ is the ratio of Lorentz Factor of proton to that of neutron and $\chi_\pi \simeq 2.15$ is the threshold for pion production (e.g. Landau & Lifshitz 1971; Koers & Giannios 2007). For the Poynting-flux-dominated (PFD) case, $m = 1/3$ and the saturation radius is much larger than the pion creation radius, $\tau_{np} \simeq 0.01\zeta_n^{1/2}$ is several times smaller than that of fireball ($\tau_{np} \simeq 0.05\text{--}0.1$). Thus, the corresponding U.L. of ξ_N is even much larger than that obtained in the fireball scenario, which seems too large for the assumption that the Poynting flux is dominated. Therefore, the U.L. can not provide a stringent constraint in the PFD scenario.

A third scenario of a hybrid jet with $1 \lesssim \sigma_0 < 10$, could be considered as well. If the decoupling occurs during the rapid acceleration, the case is similar to the fireball scenario; similar to the above discussion, the U.L. of $\xi_N \sim$ a few could be also obtained, which seems consistent with the hybrid scenario if we assume there exists a Poynting flux of which the energy is comparable with $E_{\gamma,\text{iso}}$. Otherwise, it is similar to the PFD scenario.

2.2.2. collisions in neutron-loaded flows

The pn collisions occur not only in the case of np decoupling before the coasting regime, but also in the case of internal collisions between the compound flow if Γ_{np} is larger than η and the coasting occurs earlier than the decoupling (e.g. Murase et al. 2013). As discussed in Murase et al. (2013), the energy of the produced neutrinos is

$$E_\nu^{\text{qt}} \approx 0.1\Gamma_{\text{rel}}' m_p c^2 / (1+z), \quad (32)$$

where $\Gamma_{\text{rel}}' \sim 2$ is the relative Lorentz factor of the interacting flow and sub-TeV neutrinos are expected for $\Gamma \sim 10^2\text{--}10^3$. The neutrino energy fluence is

$$E_\nu^2 \phi_{\nu_\mu} \approx \frac{1}{12} \frac{(1+z)}{4\pi d_L^2} \tau_{pn} \xi_N E_{\gamma,\text{iso}}. \quad (33)$$

Internal collisions between neutron-loaded flows may be relevant for sub-photospheric dissipation (e.g. Beloborodov 2010). $\xi_N \sim 4\text{--}20$ is predicted in this scenario (e.g. Vurm et al. 2011a). As shown in Figure 2 (c), the U.L. of ξ_N could reach up to ~ 5 with $\tau_{np} = 1$, which could be consistent with the scenario. The U.L. of $\xi_N \sim 0.5$ is obtained within the smaller constraint of U.L.=0.1 GeV cm⁻², seems too small. However, it may be reasonable for a hybrid jet in which there exists an appreciable Poynting flux, because a considerable part of $E_{\gamma,\text{iso}}$ could be contributed by the dissipation of the Poynting flux via e.g. ICMART mechanism.

2.3. Other processes: pp collisions, multi-pions and Kaons production in pp collisions and $p\gamma$ interactions

Other processes, such as pp collisions, multi-pions and kaons production in pp collisions and $p\gamma$ interactions (e.g. Wang & Dai 2009; Gao et al. 2012) could also contribute to the neutrino emission. However, compared with the estimations above, their contributions are not much larger, and do not affect the conclusion.

2.4. Implications

The U.L. (1 GeV cm²) of the neutrino fluence for GRB 230307A seems too loose to constrain a specific GRB emission mechanism, if the non-thermal neutrino production via $p\gamma$ interactions is the only consideration. For QT neutrinos, the U.L. of $\xi_N \sim$ a few, which seems higher than that ($\xi_N \lesssim 0.1$) of GRB 221009A. If the baryon loading is really appreciable, the jet is not PFD as that in GRB 221009A. Therefore, it may be necessary to directly investigate the prompt emission mechanism from spectra in the prompt phase to see if there is something different.

3. BASIC SPECTRAL PROPERTIES OF GRB 230307A

GBM NaI detector (NaI 10), and GBM BGO (BGO 1) detector recorded the brightest flux, however, dead time (DT) and pile-up instrumental (PUI) effects occur in $[T_0 + 2.5, T_0 + 11.0]$ s (GCN 33551, Dalessi & Fermi GBM Team 2023), as shown in the red shadow in the light curve in Figure 3 (a). Fortunately, data from GECAM-B are not distorted by PUI effect. Therefore, data analysis is performed with data from the brightest detector (GRD 4) of GECAM-B from $[T_0 + 2.2, T_0 + 11.7]$ s, while in other time bins, data from the two brightest detectors (NaI 10 and BGO 1) of GBM are used. A polynomial is applied to fit all the energy channels and then interpolated into the signal interval to yield the background photon count estimate for GRB data. The Markov Chain Monte Carlo (MCMC) fitting is performed to find the parameters with the maximum Poisson likelihood.

From Figure 3 (a), the values of $\alpha \gtrsim -2/3$ (synchrotron death line, Preece et al. 1998) concentrate in the first 7 s, which implies that the emission at the beginning may have a photospheric origin. The fit results are shown in Table A1 in Appendix A. After about 7 s, α gradually decreases to about -1.6, which means that the non-thermal emission may become dominant gradually afterwards. The typical QT spectra in the first few seconds are shown in Figure 3 (c)-(e), which is narrow with the maximum of $\alpha \sim -0.3$ and more like a broadened Planck spectrum after subtracting the non-thermal emission denoted by a power-law (PL) function. The photospheric emission is a natural consequence of

the fireball (e.g., Cavallo & Rees 1978; Goodman 1986; Paczynski 1986). The Planck spectrum related to the photospheric emission could be broadened by geometrical broadening (Pe'er 2008; Lundman et al. 2013), as well as by dissipations below the photosphere (e.g., Rees & Mészáros 2005), such as magnetic reconnection (e.g., Giannios & Spruit 2005), and hadronic collision shocks (e.g., Vurm et al. 2011b).

From Figure 3 (f)-(h) and the decreasing α with time, it is found that the so-called QT spectral shape becomes broader. This may be caused by the enhanced dissipation below the photosphere with time. The details of the spectral evolution are not the main goal in this letter and will not be further discussed. In summary, an significant existence of the photospheric emission is observed in the prompt phase of GRB 230307A, which is greatly different from that in GRB 221009A.

4. DISCUSSION AND SUMMARY

I. Constraints from the possible neutrino emission on GRB 230307A

$E_{\text{iso},\gamma}$ for GRB 230307A is not large enough, compared with the nearby extremely bright GRB 130427A and 221009A. The U.L. seems so loose that the emission mechanisms for this burst are not well constrained, with assuming that the neutrinos production from $p\gamma$ interactions is the only consideration. The case is similar even if the U.L. is one order smaller. It is proposed that the QT neutrinos from hadronuclear processes may contribute to the neutrino emission. The U.L. of allowed nucleon loading factor is about a few in this neutron-rich post-merger environment of GRB 230307A.

II. The nucleon loading and emission mechanism in GRB 230307A

The neutrino emission is relevant to the emission mechanism and the jet composition for GRBs. Three different jet properties are considered in the estimation for the QT neutrino fluence. The U.L. of the nucleon loading $\xi_N \sim$ a few for GRB 230307A, while the U.L. of $\xi_N \lesssim 0.1$ for GRB 221009A, which may imply that a heavier nucleon loading is allowed in GRB 230307A than that in GRB 221009A.

For GRB 221009A, the U.L. of allowed $\xi_N \lesssim 0.1$ is very small, which is consistent very well with its jet composition and emission properties inferred from the spectral modeling (Yang et al. 2023): a PFD jet (with a synchrotron-dominated prompt emission). The prompt emission of GRB 230307A seems quite different from that of GRB 221009A. A significant photospheric emission dominates the beginning of the prompt phase; the spectrum becomes broader and broader with time, which could be interpreted by enhanced sub-

photosphere dissipations via magnetic reconnection, or hadronic collisions. The dissipation via hadronic collisions could occur in a fireball or a hybrid jet, while the magnetic dissipation may happen in a hybrid or PFD jet. If the jet is PFD, it is inferred that there must be a thermalization via the magnetic dissipation below the photosphere, to interpret the observed photospheric emission.

GRB 211211A is another nearby GRB ($z = 0.076$) and has a same origin as GRB 230307A (Yang et al. 2022). There is no report about the relevant neutrino emission, however, σ_0 tells some information about the nucleon loading. $\sigma_0 \sim 10\text{--}100$ is estimated for GRB 211211A (Chang et al. 2023). This means that the jet for GRB 211211A is PFD and nucleon loading is small. Besides, there exist neither significant photospheric emissions, nor evident spectral evolution (from photospheric to non-thermal) in the prompt phase. It may be inferred that the jet composition of GRB 230307A is somewhat different from those of GRB 211211A and GRB 221009A, and a heavier baryon loading may account for it.

III. Assuming a more stringent constraint from neutrinos detection

A data set of high-energy track events are used in the analysis by IceCube to extract the U.L. of neutrino fluence, and the sensitivity can vary greatly over different declinations (δ) (Abbasi et al. 2021, 2023b). GRB 230307A is located at the southern hemisphere with $\delta = -75.4^\circ$, while $\delta = +19.8^\circ$ for GRB 221009A. The U.L. for non-detection in GRB 230307A might be about one order of magnitude lower if it was in northern hemisphere with a reduced background. Thus, with assuming that it has the same sensitivity as that in the northern hemisphere, 0.1 GeV cm^{-2} as a U.L. is also used in the analysis as shown in Section 2. However, this smaller U.L. still can not provide a stringent constraint on GRB emission mechanisms via $p\gamma$ interactions, as shown in Figure 2. For the QT neutrino emission, a smaller U.L. is obtained, however, it is still much larger than that in GRB 221009A or GRB 211211A. The conclusion is similar to that with 1 GeV cm^{-2} as a U.L..

We note that till now no GRB-neutrinos have been ever detected, even for the two brightest nearby GRBs ever observed (GRB 221009A and GRB 230307A), which have different representative dissipation mechanisms. There may be some hints that: only a brighter and/or more nearby GRB might be expected for the detection for the candidate of the source of GRB-neutrinos; for the future neutrino detectors, sub-TeV channels and relevant dedicated searches with considering

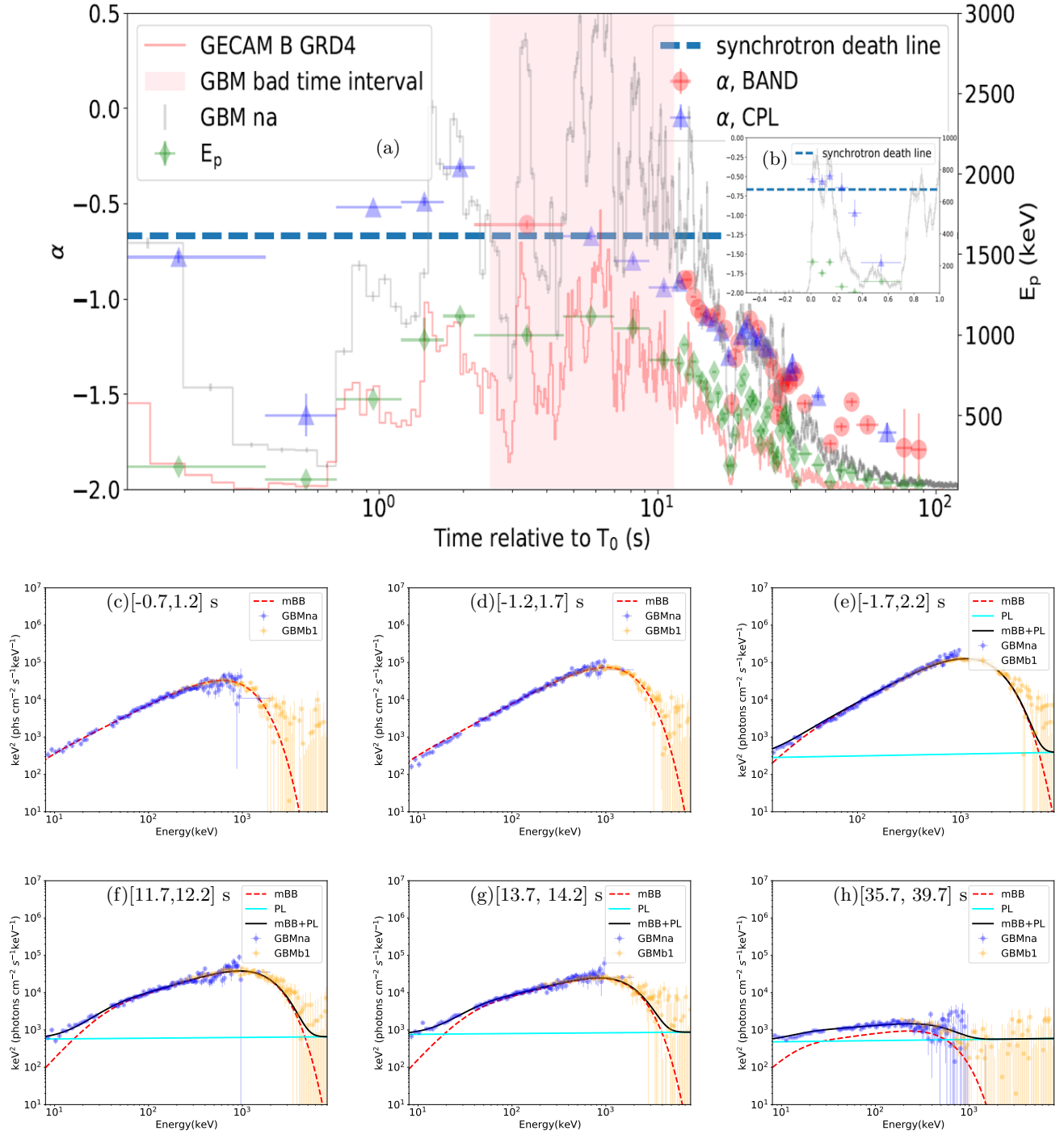


Figure 3. (a) The light curves (logarithm scale) of GBM na detector and α , E_p values, with a sub-plot (b) for the first 1 s. Red circles and blue triangles denote α values from the fit results with BAND and CPL functions (the same below), respectively. Green diamonds denote the E_p values from the fit results. The sub-plot shows α and E_p values of the first 1 s. (c)-(h) Time resolved spectra with modeling with multi-blackbody (mBB) or mBB+PL functions.

the neutrino spectrum shape are of great importance.

1 The authors thank supports from the National Pro-
 2 gram on Key Research and Development Project
 3 (2021YFA0718500) and National Natural Science Foun-
 4 dation of China (grant Nos. 12303052). This
 5 work is partially supported by International Partner-
 6 ship Program of Chinese Academy of Sciences (Grant
 7 No.113111KYSB20190020). The author is very grate-
 8 ful to the suggestions from Jessie Thwaites and the Ice-
 9 Cube Collaboration. Dr. Xin-Ying Song thanks public
 10 GRB data of Fermi/GBM and GECAM-B data group.
 11 I am very grateful for the comments and suggestions
 12 from the anonymous referees. I thank Dr. Rui Qiao for
 13 his suggestions on the response matrix generating for
 14 GECAM-B data. I thank Dr. Michael S. Briggers and
 15 Dr. Michelle Hui for their suggestions on GBM data. I
 16 thank Dr. Xi-Lu Wang and Prof. Shuang-Nan Zhang
 17 for their suggestions.

APPENDIX

A. THE FIT RESULTS OF THE PROMPT EMISSION OF GRB 230307A

The fit results modeling with mBB or mBB+PL models and empirical functions are listed in Table. [A1](#).

Table A1. The time-resolved results with mBB, mBB+PL and BAND functions.

Time bins	Favoured or Used Model	m	kT_{\min}	kT_{\max}	F_T	α	F_{NT}	BIC	$\frac{\chi^2}{\text{ndof}}$
(s)			(keV)	(keV)	(10^{-6} erg cm^{-2} s^{-1})		(10^{-6} erg cm^{-2} s^{-1})		
[-0.01, 0.39]	mBB+PL	$-0.35^{+0.07}_{-0.09}$	$5.9^{+0.7}_{-0.4}$	$105.2^{+7.0}_{-5.2}$	$30.3^{+0.5}_{-0.4}$			249.0	$\frac{239.7}{207}$
		$-0.44^{+0.09}_{-0.09}$	$8.5^{+1.2}_{-1.2}$	$108.5^{+50.6}_{-20.0}$	$27.2^{+1.8}_{-1.2}$	$-2.09^{+0.05}_{-0.01}$	$7.0^{+7.2}_{-2.5}$	235.6	$\frac{221.6}{205}$
[0.39, 0.7]	BAND	α	β	E_{p}			$5.89^{+0.89}_{-0.61}$	122.3	$\frac{113.6}{147}$
[0.7, 1.2]	mBB	$0.30^{+0.02}_{-0.03}$	$1.9^{+1.0}_{-0.6}$	$259.9^{+5.2}_{-4.6}$	$106.6^{+1.1}_{-1.5}$			250.2	$\frac{241.6}{236}$
		$0.24^{+0.03}_{-0.03}$	$13.4^{+1.6}_{-1.6}$	$268.5^{+8.6}_{-7.3}$	$103.0^{+1.3}_{-1.6}$	$-1.97^{+0.03}_{-0.02}$	$7.5^{+1.1}_{-1.1}$	254.9	$\frac{240.6}{234}$
[1.2, 1.7]	mBB	$0.35^{+0.01}_{-0.03}$	$1.8^{+0.9}_{-0.5}$	$418.3^{+6.0}_{-5.6}$	$232.3^{+2.7}_{-1.6}$			222.2	$\frac{212.7}{236}$
		$0.38^{+0.03}_{-0.02}$	$8.5^{+2.1}_{-1.4}$	$413.2^{+6.7}_{-6.2}$	$229.4^{+3.7}_{-3.1}$	$-1.95^{+0.05}_{-0.03}$	$6.0^{+1.0}_{-1.1}$	228.9	$\frac{214.6}{234}$
[1.7, 2.2]	mBB+PL	$0.53^{+0.01}_{-0.01}$	$1.6^{+0.6}_{-0.4}$	$462.9^{+5.5}_{-4.7}$	$382.0^{+4.3}_{-2.5}$			333.6	$\frac{324.1}{236}$
		$0.64^{+0.03}_{-0.03}$	$9.0^{+4.1}_{-3.2}$	$445.3^{+6.7}_{-20.0}$	$374.7^{+3.6}_{-3.6}$	$-1.95^{+0.03}_{-0.05}$	$8.4^{+2.0}_{-2.5}$	302.1	$\frac{287.8}{234}$
[2.2, 4.6]	mBB+PL	$0.18^{+0.02}_{-0.02}$	$10.0^{+7.3}_{-0.7}$	$439.1^{+127.0}_{-15.7}$	$270.3^{+115.9}_{-6.3}$			269.1	$\frac{259.7}{220}$
		$0.21^{+0.03}_{-0.03}$	$11.0^{+2.2}_{-1.8}$	$431.4^{+20.0}_{-15.0}$	$263.1^{+7.5}_{-7.5}$	$-1.98^{+0.20}_{-0.11}$	$6.9^{+10.0}_{-5.5}$	268.7	$\frac{254.6}{218}$
[4.6, 7.0]	mBB+PL	$0.14^{+0.03}_{-0.04}$	$10.0^{+4.8}_{-0.6}$	$492.0^{+33.0}_{-16.9}$	$394.6^{+15.6}_{-8.6}$			283.5	$\frac{274.1}{220}$
		$0.16^{+0.10}_{-0.04}$	$12.5^{+1.5}_{-1.5}$	$493.4^{+126.0}_{-21.0}$	$385.9^{+13.6}_{-17.8}$	$-1.98^{+0.37}_{-0.05}$	$15.8^{+13.0}_{-10.4}$	282.9	$\frac{268.8}{218}$
[7.0, 9.3]	mBB+PL	$-0.03^{+0.03}_{-0.19}$	$10.5^{+3.3}_{-0.6}$	$507.3^{+110.0}_{-22.1}$	$271.0^{+73.0}_{-6.1}$			311.6	$\frac{302.2}{220}$
		$-0.02^{+0.03}_{-0.04}$	$11.4^{+1.9}_{-0.9}$	$506.4^{+40.0}_{-20.0}$	$265.4^{+5.9}_{-5.9}$	$-1.98^{+0.20}_{-0.40}$	$8.0^{+8.5}_{-7.7}$	310.6	$\frac{296.5}{218}$
[9.3, 11.7]	mBB+PL	$-0.23^{+0.03}_{-0.21}$	$10.7^{+1.5}_{-0.5}$	$491.8^{+110.0}_{-30.3}$	$177.0^{+60.1}_{-3.1}$			270.7	$\frac{261.3}{220}$
		$-0.22^{+0.02}_{-0.04}$	$11.5^{+4.1}_{-0.8}$	$490.7^{+80.0}_{-52.1}$	$171.5^{+11.1}_{-8.4}$	$-1.99^{+0.20}_{-0.32}$	$9.4^{+10.0}_{-7.6}$	267.7	$\frac{253.6}{218}$
[2.2, 11.7]	mBB+PL	$0.03^{+0.01}_{-0.01}$	$10.1^{+0.4}_{-0.3}$	$504.4^{+13.6}_{-10.5}$	$288.2^{+4.2}_{-3.8}$			340.0	$\frac{330.6}{220}$
		$0.04^{+0.02}_{-0.05}$	$10.9^{+25.1}_{-0.8}$	$502.9^{+12.0}_{-10.0}$	$281.9^{+4.1}_{-4.1}$	$-2.03^{+0.43}_{-0.15}$	$12.8^{+10.0}_{-10.0}$	319.3	$\frac{305.2}{218}$
[11.7, 12.2]	mBB+PL	$-0.18^{+0.02}_{-0.02}$	$6.5^{+0.4}_{-0.4}$	$454.2^{+12.9}_{-12.1}$	$151.8^{+2.0}_{-2.0}$			298.2	$\frac{288.6}{236}$
		$-0.19^{+0.01}_{-0.03}$	$9.8^{+0.7}_{-0.7}$	$461.5^{+10.0}_{-10.0}$	$146.2^{+1.9}_{-1.9}$	$-1.98^{+0.02}_{-0.02}$	$9.3^{+1.5}_{-1.7}$	291.8	$\frac{277.5}{234}$
[12.2, 12.7]	mBB+PL	$-0.14^{+0.02}_{-0.02}$	$6.1^{+0.4}_{-0.4}$	$486.2^{+12.1}_{-11.9}$	$160.0^{+2.0}_{-2.0}$			258.3	$\frac{248.8}{236}$
		$-0.15^{+0.02}_{-0.02}$	$9.7^{+0.7}_{-0.7}$	$491.5^{+13.2}_{-12.6}$	$154.6^{+2.4}_{-2.4}$	$-1.97^{+0.01}_{-0.01}$	$9.3^{+1.7}_{-2.0}$	256.2	$\frac{241.9}{234}$
[12.7, 13.2]	mBB+PL	$-0.17^{+0.02}_{-0.02}$	$6.5^{+0.3}_{-0.3}$	$409.2^{+9.9}_{-9.6}$	$178.4^{+2.0}_{-2.3}$			305.4	$\frac{295.8}{236}$
		$-0.20^{+0.02}_{-0.02}$	$10.2^{+0.5}_{-0.9}$	$419.8^{+10.6}_{-10.5}$	$171.7^{+2.6}_{-2.6}$	$-1.98^{+0.02}_{-0.01}$	$11.9^{+1.8}_{-1.7}$	299.8	$\frac{276.5}{234}$
[13.2, 13.7]	mBB+PL	$-0.23^{+0.01}_{-0.01}$	$5.7^{+0.3}_{-0.3}$	$469.9^{+13.6}_{-12.7}$	$148.9^{+2.0}_{-1.9}$			299.0	$\frac{289.5}{236}$
		$-0.23^{+0.02}_{-0.01}$	$7.8^{+0.9}_{-0.9}$	$470.1^{+14.9}_{-16.2}$	$143.3^{+2.9}_{-2.7}$	$-1.97^{+0.02}_{-0.02}$	$8.6^{+2.1}_{-2.3}$	298.8	$\frac{284.6}{234}$
[13.7, 14.2]	mBB+PL	$-0.30^{+0.02}_{-0.02}$	$5.8^{+0.3}_{-0.4}$	$433.1^{+19.5}_{-13.9}$	$106.3^{+1.2}_{-2.3}$			238.8	$\frac{229.3}{236}$
		$-0.31^{+0.02}_{-0.02}$	$9.8^{+0.8}_{-0.8}$	$441.0^{+16.8}_{-16.0}$	$99.3^{+1.3}_{-1.3}$	$-1.98^{+0.04}_{-0.01}$	$12.2^{+1.5}_{-1.6}$	215.5	$\frac{201.2}{234}$
[14.2, 14.7]	mBB+PL	$-0.34^{+0.02}_{-0.01}$	$5.5^{+0.3}_{-0.2}$	$442.3^{+17.6}_{-16.6}$	$105.4^{+2.0}_{-2.0}$			260.7	$\frac{251.2}{236}$
		$-0.35^{+0.03}_{-0.02}$	$9.0^{+0.9}_{-0.7}$	$449.7^{+23.8}_{-15.8}$	$97.9^{+2.7}_{-1.4}$	$-1.99^{+0.02}_{-0.01}$	$13.1^{+1.7}_{-1.7}$	240.3	$\frac{226.0}{234}$
[14.7, 15.2]	mBB+PL	$-0.36^{+0.02}_{-0.02}$	$5.6^{+0.3}_{-0.3}$	$415.5^{+15.8}_{-15.1}$	$103.5^{+1.2}_{-1.2}$			240.7	$\frac{231.2}{234}$
		$-0.36^{+0.02}_{-0.03}$	$7.0^{+0.8}_{-0.7}$	$417.2^{+17.1}_{-16.0}$	$99.6^{+1.3}_{-2.7}$	$-2.03^{+0.03}_{-0.02}$	$7.0^{+2.6}_{-2.4}$	239.4	$\frac{225.2}{232}$
[15.2, 15.7]	mBB+PL	$-0.34^{+0.02}_{-0.02}$	$5.0^{+0.2}_{-0.5}$	$352.2^{+14.6}_{-14.6}$	$82.1^{+1.4}_{-1.4}$			271.0	$\frac{261.5}{234}$
		$-0.34^{+0.02}_{-0.03}$	$7.7^{+0.4}_{-0.8}$	$353.9^{+15.1}_{-15.4}$	$76.1^{+1.9}_{-1.4}$	$-1.98^{+0.02}_{-0.01}$	$10.4^{+1.8}_{-2.1}$	262.0	$\frac{247.7}{232}$
	BAND	α	β	E_{peak}					
[-0.01, 0.39]	BAND	$-0.77^{+0.02}_{-0.02}$	$-7.43^{+2.80}_{-0.47}$	$180.7^{+4.3}_{-4.4}$			$31.3^{+0.6}_{-0.3}$	243.30	$\frac{234.0}{207}$
[0.39, 0.7]	BAND	$-1.56^{+0.07}_{-0.11}$	$-6.88^{+3.66}_{-3.49}$	$98.3^{+17.0}_{-26.5}$			$5.8^{+0.9}_{-0.6}$	126.59	$\frac{117.9}{147}$
[0.7, 1.2]	BAND	$-0.52^{+0.03}_{-0.00}$	$-8.98^{+3.62}_{-1.50}$	$599.9^{+10.3}_{-2.4}$			$109.0^{+0.10}_{-0.90}$	248.78	$\frac{239.3}{236}$
[1.2, 1.7]	BAND	$-0.49^{+0.01}_{-0.03}$	$-11.94^{+2.00}_{-3.58}$	$968.9^{+8.5}_{-7.2}$			$233.2^{+1.8}_{-2.4}$	265.97	$\frac{256.5}{236}$
[1.7, 2.2]	BAND	$-0.31^{+0.01}_{-0.03}$	$-9.40^{+2.90}_{-9.87}$	$1117.4^{+17.1}_{-10.0}$			$382.5^{+6.2}_{-3.6}$	417.51	$\frac{408.0}{236}$
[2.2, 4.575]	BAND	$-0.61^{+0.02}_{-0.02}$	$-7.28^{+3.13}_{-3.00}$	$998.4^{+41.7}_{-34.0}$			$278.3^{+5.1}_{-6.6}$	280.20	$\frac{270.8}{220}$
[4.575, 6.95]	BAND	$-0.67^{+0.01}_{-0.02}$	$-7.36^{+10.34}_{-3.00}$	$1115.0^{+26.1}_{-26.1}$			$412.1^{+4.6}_{-8.2}$	297.46	$\frac{288.1}{220}$
[6.95, 9.325]	BAND	$-0.80^{+0.01}_{-0.02}$	$-7.21^{+3.10}_{-3.00}$	$1037.8^{+44.5}_{-29.7}$			$279.9^{+9.8}_{-7.5}$	330.89	$\frac{321.5}{220}$
[9.325, 11.7]	BAND	$-0.94^{+0.02}_{-0.02}$	$-6.70^{+0.13}_{-0.13}$	$838.3^{+38.0}_{-44.0}$			$178.92^{+5.3}_{-10.0}$	295.42	$\frac{286.0}{220}$

Table. A1— Continued.

Time bins	Favoured or Used Model	α	β	E_{peak}	F_{NT}	BIC	$\frac{\chi^2}{ndof}$
(s)				(keV)	(10^{-6} erg cm^{-2} s^{-1})		
[11.7, 12.2]	BAND	-0.92 ^{+0.03} _{-0.01}	-8.12 ^{+3.82} _{-5.67}	872.7 ^{+76.9} _{-0.0}	154.3 ^{+2.7} _{-0.0}	331.96	322.4 ₂₃₆
[12.2, 12.7]	BAND	-0.90 ^{+0.05} _{-0.02}	-9.61 ^{+2.32} _{-7.22}	939.0 ^{+10.6} _{-7.1}	159.9 ^{+2.0} _{-2.5}	278.60	269.1 ₂₃₆
[12.7, 13.2]	BAND	-0.90 ^{+0.01} _{-0.01}	-10.87 ^{+1.07} _{-8.34}	756.7 ^{+6.3} _{-11.6}	180.7 ^{+3.3} _{-4.1}	315.01	305.5 ₂₃₆
[13.2, 13.7]	BAND	-0.99 ^{+0.01} _{-0.01}	-9.08 ^{+3.72} _{-6.08}	835.7 ^{+10.0} _{-10.0}	149.2 ^{+1.1} _{-2.3}	314.46	304.9 ₂₃₆
[13.7, 14.2]	BAND	-1.05 ^{+0.01} _{-0.01}	-10.71 ^{+1.23} _{-8.51}	742.5 ^{+5.2} _{-7.9}	107.8 ^{+1.4} _{-1.4}	291.45	281.9 ₂₃₆
[14.2, 14.7]	BAND	-1.09 ^{+0.01} _{-0.02}	-8.61 ^{+3.14} _{-6.39}	722.0 ^{+9.0} _{-5.0}	106.9 ^{+1.2} _{-1.2}	254.52	245.0 ₂₃₆
[14.7, 15.2]	BAND	-1.08 ^{+0.01} _{-0.03}	-8.74 ^{+3.20} _{-2.46}	657.0 ^{+12.5} _{-10.4}	104.2 ^{+1.2} _{-1.2}	284.62	275.1 ₂₃₆
[15.2, 15.7]	BAND	-1.09 ^{+0.01} _{-0.02}	-8.55 ^{+9.56} _{-7.47}	586.1 ^{+17.0} _{-20.0}	84.1 ^{+1.4} _{-0.7}	284.59	275.1 ₂₃₆
[15.7, 16.2]	BAND	-1.12 ^{+0.01} _{-0.02}	-8.61 ^{+2.00} _{-2.71}	793.3 ^{+28.9} _{-19.3}	89.4 ^{+1.8} _{-1.2}	281.45	271.9 ₂₃₆
[16.2, 16.7]	BAND	-1.07 ^{+0.02} _{-0.03}	-8.40 ^{+2.73} _{-2.98}	685.5 ^{+20.0} _{-93.3}	81.3 ^{+1.5} _{-1.0}	267.13	257.6 ₂₃₆
[16.7, 17.2]	BAND	-1.17 ^{+0.01} _{-0.06}	-8.44 ^{+2.37} _{+3.86}	481.6 ^{+20.0} _{-22.1}	49.7 ^{+0.6} _{-1.2}	266.30	256.8 ₂₃₆
[17.2, 17.7]	BAND	-1.16 ^{+0.06} _{-0.01}	-8.27 ^{+3.56} _{-2.00}	511.5 ^{+22.1} _{-14.7}	48.8 ^{+1.2} _{-0.6}	199.33	189.8 ₂₃₆
[17.7, 18.2]	BAND	-1.29 ^{+0.05} _{-0.03}	-7.58 ^{+0.12} _{-2.10}	197.6 ^{+28.3} _{-11.6}	13.1 ^{+0.3} _{-0.5}	243.51	234.0 ₂₃₆
[18.2, 18.7]	BAND	-1.55 ^{+0.06} _{-0.02}	-7.06 ^{+3.06} _{-3.00}	219.6 ^{+32.4} _{-39.3}	10.9 ^{+0.6} _{-0.8}	184.64	175.1 ₂₃₆
[18.7, 19.2]	BAND	-1.30 ^{+0.03} _{-0.03}	-7.75 ^{+3.05} _{-2.90}	380.0 ^{+39.0} _{-20.0}	30.6 ^{+0.6} _{-0.6}	204.36	194.8 ₂₃₆
[19.2, 19.7]	BAND	-1.23 ^{+0.02} _{-0.02}	-8.40 ^{+2.63} _{-2.00}	504.9 ^{+20.0} _{-26.1}	56.8 ^{+0.9} _{-0.9}	264.82	255.3 ₂₃₆
[19.7, 20.2]	BAND	-1.22 ^{+0.01} _{-0.01}	-8.70 ^{+0.87} _{-8.07}	715.6 ^{+12.5} _{-10.4}	78.7 ^{+1.7} _{-1.1}	308.10	298.6 ₂₃₆
[20.2, 20.7]	BAND	-1.16 ^{+0.03} _{-0.01}	-8.48 ^{+3.21} _{-3.20}	730.0 ^{+17.2} _{-9.1}	70.3 ^{+1.4} _{-1.4}	292.01	282.5 ₂₃₆
[20.7, 21.2]	BAND	-1.12 ^{+0.02} _{-0.00}	-8.38 ^{+9.56} _{-0.25}	526.2 ^{+25.1} _{-18.8}	54.6 ^{+1.1} _{-1.1}	280.33	270.8 ₂₃₆
[21.2, 21.7]	BAND	-1.12 ^{+0.03} _{-0.00}	-8.31 ^{+5.21} _{-4.19}	593.3 ^{+20.0} _{-20.0}	71.8 ^{+1.1} _{-1.1}	267.21	257.7 ₂₃₆
[21.7, 22.2]	BAND	-1.19 ^{+0.02} _{-0.02}	-8.51 ^{+2.36} _{-7.45}	561.1 ^{+24.0} _{-24.0}	51.5 ^{+0.9} _{-0.9}	239.74	230.2 ₂₃₆
[22.2, 22.7]	BAND	-1.21 ^{+0.00} _{-0.03}	-8.44 ^{+3.12} _{-6.50}	545.2 ^{+20.0} _{-20.0}	45.6 ^{+0.7} _{-0.7}	240.01	230.5 ₂₃₆
[22.7, 23.2]	BAND	-1.15 ^{+0.00} _{-0.03}	-7.95 ^{+2.86} _{-3.03}	405.4 ^{+20.0} _{-20.0}	41.1 ^{+0.7} _{-0.7}	221.29	211.8 ₂₃₆
[23.2, 23.7]	BAND	-1.18 ^{+0.00} _{-0.03}	-7.73 ^{+3.87} _{-3.03}	292.0 ^{+10.0} _{-10.0}	28.9 ^{+0.7} _{-0.7}	226.04	216.5 ₂₃₆
[23.7, 24.2]	BAND	-1.26 ^{+0.02} _{-0.01}	-8.09 ^{+9.75} _{-0.00}	406.7 ^{+16.0} _{-21.4}	40.2 ^{+0.9} _{-0.9}	270.98	261.5 ₂₃₆
[24.2, 24.7]	BAND	-1.29 ^{+0.01} _{-0.01}	-8.31 ^{+2.72} _{-3.19}	505.9 ^{+23.4} _{-31.2}	44.5 ^{+0.5} _{-1.1}	256.69	247.2 ₂₃₆
[24.7, 25.2]	BAND	-1.25 ^{+0.02} _{-0.01}	-8.00 ^{+2.00} _{-2.00}	526.2 ^{+21.2} _{-28.2}	44.5 ^{+1.2} _{-1.0}	230.45	220.9 ₂₃₆
[25.2, 25.7]	BAND	-1.31 ^{+0.03} _{-0.02}	-8.25 ^{+3.36} _{-6.46}	340.8 ^{+16.0} _{-16.0}	41.8 ^{+0.7} _{-0.7}	266.04	256.5 ₂₃₆
[25.7, 26.2]	BAND	-1.37 ^{+0.02} _{-0.03}	-7.97 ^{+9.83} _{-0.03}	271.0 ^{+12.3} _{-9.3}	31.9 ^{+0.7} _{-0.4}	228.73	219.2 ₂₃₆
[26.2, 26.7]	BAND	-1.48 ^{+0.02} _{-0.02}	-7.20 ^{+4.24} _{-2.10}	192.4 ^{+15.1} _{-10.8}	24.1 ^{+0.5} _{-0.5}	195.13	185.6 ₂₃₆
[26.7, 27.2]	BAND	-1.61 ^{+0.03} _{-0.03}	-7.11 ^{+3.20} _{-3.30}	240.7 ^{+66.7} _{-32.7}	25.4 ^{+1.0} _{-1.0}	259.15	249.6 ₂₃₆
[27.2, 27.7]	BAND	-1.54 ^{+0.03} _{-0.01}	-7.69 ^{+2.10} _{-3.60}	404.0 ^{+8.1} _{-13.2}	26.4 ^{+0.9} _{-0.6}	240.60	231.1 ₂₃₆
[27.7, 28.2]	BAND	-1.44 ^{+0.01} _{-0.03}	-8.28 ^{+0.37} _{-9.50}	453.9 ^{+10.6} _{-4.1}	37.3 ^{+0.6} _{-1.2}	203.75	194.2 ₂₃₆
[28.2, 28.7]	BAND	-1.41 ^{+0.03} _{-0.01}	-7.76 ^{+1.20} _{-2.08}	528.9 ^{+21.1} _{-10.4}	40.7 ^{+0.9} _{-0.9}	233.97	224.4 ₂₃₆
[28.7, 29.2]	BAND	-1.44 ^{+0.00} _{-0.02}	-7.38 ^{+0.80} _{-3.20}	516.8 ^{+45.7} _{-45.7}	24.2 ^{+1.1} _{-0.7}	232.61	223.1 ₂₃₆
[29.2, 29.7]	BAND	-1.45 ^{+0.02} _{-0.02}	-7.71 ^{+0.70} _{-1.20}	394.2 ^{+0.6} _{-58.4}	19.0 ^{+0.6} _{-0.8}	215.80	206.3 ₂₃₆
[29.7, 30.2]	BAND	-1.43 ^{+0.01} _{-0.03}	-8.26 ^{+9.87} _{-0.00}	510.1 ^{+43.1} _{-43.1}	24.9 ^{+1.0} _{-0.8}	220.93	211.4 ₂₃₆
[30.2, 30.7]	BAND	-1.33 ^{+0.03} _{-0.03}	-7.16 ^{+2.10} _{-1.20}	266.1 ^{+6.0} _{-2.0}	13.2 ^{+0.4} _{-0.6}	222.34	212.8 ₂₃₆
[30.7, 31.2]	BAND	-1.38 ^{+0.03} _{-0.03}	-7.22 ^{+3.00} _{-2.00}	211.0 ^{+7.2} _{-3.2}	11.6 ^{+0.4} _{-0.4}	196.71	187.2 ₂₃₆
[31.2, 31.7]	BAND	-1.40 ^{+0.06} _{-0.06}	-7.18 ^{+3.00} _{-3.12}	149.2 ^{+12.0} _{-19.7}	9.4 ^{+0.4} _{-0.4}	177.98	168.5 ₂₃₆
[31.7, 35.7]	BAND	-1.55 ^{+0.02} _{-0.02}	-7.98 ^{+5.42} _{-1.69}	254.5 ^{+9.0} _{-9.0}	14.9 ^{+0.2} _{-0.2}	300.80	291.3 ₂₃₆
[35.7, 39.7]	BAND	-1.51 ^{+0.02} _{-0.00}	-7.89 ^{+9.76} _{-0.00}	192.8 ^{+8.2} _{-10.1}	10.4 ^{+0.1} _{-0.1}	255.69	246.2 ₂₃₆
[39.7, 43.7]	BAND	-1.76 ^{+0.02} _{-0.02}	-7.10 ^{+3.00} _{-3.40}	125.3 ^{+10.0} _{-10.0}	7.5 ^{+1.1} _{-1.0}	185.46	175.9 ₂₃₆
[43.7, 47.7]	BAND	-1.67 ^{+0.02} _{-0.02}	-7.49 ^{+3.00} _{-3.00}	162.8 ^{+9.1} _{-13.8}	6.7 ^{+0.5} _{-0.5}	176.36	166.8 ₂₃₆
[47.7, 51.7]	BAND	-1.54 ^{+0.02} _{-0.02}	-7.19 ^{+2.40} _{-1.22}	142.7 ^{+11.1} _{-4.9}	4.8 ^{+0.0} _{-0.2}	186.30	176.8 ₂₃₆
[51.7, 61.7]	BAND	-1.67 ^{+0.03} _{-0.03}	-7.64 ^{+3.99} _{-5.74}	88.1 ^{+12.1} _{-6.5}	3.5 ^{+0.2} _{-0.2}	163.82	154.3 ₂₃₆
[61.7, 71.7]	BAND	-1.70 ^{+0.03} _{-0.05}	-7.22 ^{+3.00} _{-0.12}	98.3 ^{+8.0} _{-7.0}	2.4 ^{+0.0} _{-0.0}	168.22	158.7 ₂₃₆
[71.7, 81.7]	BAND	-1.77 ^{+0.20} _{-0.10}	-6.92 ^{+3.00} _{-0.12}	43.2 ^{+10.0} _{-12.0}	1.3 ^{+0.5} _{-0.2}	143.93	134.4 ₂₃₆
[81.7, 91.7]	BAND	-1.79 ^{+0.19} _{-0.10}	-7.22 ^{+5.49} _{-2.70}	46.5 ^{+10.0} _{-10.0}	1.3 ^{+0.1} _{-0.4}	157.30	147.8 ₂₃₆

REFERENCES

- Aartsen, M. G., Ackermann, M., Adams, J., et al. 2017, *ApJ*, 843, 112, doi: [10.3847/1538-4357/aa7569](https://doi.org/10.3847/1538-4357/aa7569)
- Abbasi, R., Ackermann, M., Adams, J., et al. 2021, *ApJ*, 910, 4, doi: [10.3847/1538-4357/abe123](https://doi.org/10.3847/1538-4357/abe123)
- . 2023a, *ApJ*, 951, 45, doi: [10.3847/1538-4357/acd2ca](https://doi.org/10.3847/1538-4357/acd2ca)
- . 2023b, *ApJL*, 946, L26, doi: [10.3847/2041-8213/acc077](https://doi.org/10.3847/2041-8213/acc077)
- Ai, S., & Gao, H. 2023, *ApJ*, 944, 115, doi: [10.3847/1538-4357/acb3bf](https://doi.org/10.3847/1538-4357/acb3bf)
- Aimuratov, Y., Becerra, L. M., Bianco, C. L., et al. 2023, *The Astrophysical Journal*, 955, 93, doi: [10.3847/1538-4357/ace721](https://doi.org/10.3847/1538-4357/ace721)
- Bahcall, J. N., & Mészáros, P. 2000, *PhRvL*, 85, 1362, doi: [10.1103/PhysRevLett.85.1362](https://doi.org/10.1103/PhysRevLett.85.1362)
- Bartos, I., Beloborodov, A. M., Hurley, K., & Márka, S. 2013, *PhRvL*, 110, 241101, doi: [10.1103/PhysRevLett.110.241101](https://doi.org/10.1103/PhysRevLett.110.241101)
- Beloborodov, A. M. 2003, *ApJ*, 588, 931, doi: [10.1086/374217](https://doi.org/10.1086/374217)
- . 2010, *MNRAS*, 407, 1033, doi: [10.1111/j.1365-2966.2010.16770.x](https://doi.org/10.1111/j.1365-2966.2010.16770.x)
- Bulla, M., Camisasca, A. E., Guidorzi, C., et al. 2023, *GRB Coordinates Network*, 33578, 1
- Cavallo, G., & Rees, M. J. 1978, *MNRAS*, 183, 359, doi: [10.1093/mnras/183.3.359](https://doi.org/10.1093/mnras/183.3.359)
- Chang, X.-Z., Lü, H.-J., Yang, X., Chen, J.-M., & Liang, E.-W. 2023, *ApJ*, 943, 146, doi: [10.3847/1538-4357/aca969](https://doi.org/10.3847/1538-4357/aca969)
- Dalessi, S., & Fermi GBM Team. 2023, *GRB Coordinates Network*, 33551, 1
- Fermi GBM Team. 2023, *GRB Coordinates Network*, 33405, 1
- Gao, S., Asano, K., & Mészáros, P. 2012, *JCAP*, 2012, 058, doi: [10.1088/1475-7516/2012/11/058](https://doi.org/10.1088/1475-7516/2012/11/058)
- Gehrels, N., Norris, J. P., Barthelmy, S. D., et al. 2006, *Nature*, 444, 1044, doi: [10.1038/nature05376](https://doi.org/10.1038/nature05376)
- Giannios, D., & Spruit, H. C. 2005, *A&A*, 430, 1, doi: [10.1051/0004-6361:20047033](https://doi.org/10.1051/0004-6361:20047033)
- Goodman, J. 1986, *ApJL*, 308, L47, doi: [10.1086/184741](https://doi.org/10.1086/184741)
- Hümmer, S., Baerwald, P., & Winter, W. 2012, *PhRvL*, 108, 231101, doi: [10.1103/PhysRevLett.108.231101](https://doi.org/10.1103/PhysRevLett.108.231101)
- IceCube Collaboration. 2022, *GRB Coordinates Network*, 32665, 1
- . 2023, *GRB Coordinates Network*, 33430, 1
- Kimura, S. S. 2022, arXiv e-prints, arXiv:2202.06480, doi: [10.48550/arXiv.2202.06480](https://doi.org/10.48550/arXiv.2202.06480)
- Kimura, S. S., Murase, K., Bartos, I., et al. 2018, *PhRvD*, 98, 043020, doi: [10.1103/PhysRevD.98.043020](https://doi.org/10.1103/PhysRevD.98.043020)
- Koers, H. B. J., & Giannios, D. 2007, *A&A*, 471, 395, doi: [10.1051/0004-6361:20077560](https://doi.org/10.1051/0004-6361:20077560)
- Landau, L. D., & Lifshitz, E. M. 1971, *The classical theory of fields*
- Levan, A., Gompertz, B. P., Salafia, O. S., et al. 2023a, arXiv e-prints, arXiv:2307.02098, doi: [10.48550/arXiv.2307.02098](https://doi.org/10.48550/arXiv.2307.02098)
- Levan, A. J., Gompertz, B. P., Malesani, D. B., et al. 2023b, *GRB Coordinates Network*, 33569, 1
- Lundman, C., Pe’er, A., & Ryde, F. 2013, *MNRAS*, 428, 2430, doi: [10.1093/mnras/sts219](https://doi.org/10.1093/mnras/sts219)
- Mészáros, P., & Waxman, E. 2001, *PhRvL*, 87, 171102, doi: [10.1103/PhysRevLett.87.171102](https://doi.org/10.1103/PhysRevLett.87.171102)
- Murase, K., & Ioka, K. 2013, *PhRvL*, 111, 121102, doi: [10.1103/PhysRevLett.111.121102](https://doi.org/10.1103/PhysRevLett.111.121102)
- Murase, K., Kashiyama, K., & Mészáros, P. 2013, *PhRvL*, 111, 131102, doi: [10.1103/PhysRevLett.111.131102](https://doi.org/10.1103/PhysRevLett.111.131102)
- Murase, K., Mukhopadhyay, M., Kheirandish, A., Kimura, S. S., & Fang, K. 2022, *ApJL*, 941, L10, doi: [10.3847/2041-8213/aca3ae](https://doi.org/10.3847/2041-8213/aca3ae)
- O’Connor, B., Dichiaro, S., Troja, E., et al. 2023, *GRB Coordinates Network*, 33447, 1
- Paczynski, B. 1986, *ApJL*, 308, L43, doi: [10.1086/184740](https://doi.org/10.1086/184740)
- Paczynski, B., & Xu, G. 1994, *ApJ*, 427, 708, doi: [10.1086/174178](https://doi.org/10.1086/174178)
- Pe’er, A. 2008, *ApJ*, 682, 463, doi: [10.1086/588136](https://doi.org/10.1086/588136)
- Pe’er, A., Barlow, H., O’Mahony, S., et al. 2015, *ApJ*, 813, 127, doi: [10.1088/0004-637X/813/2/127](https://doi.org/10.1088/0004-637X/813/2/127)
- Pitik, T., Tamborra, I., & Petropoulou, M. 2021, *JCAP*, 2021, 034, doi: [10.1088/1475-7516/2021/05/034](https://doi.org/10.1088/1475-7516/2021/05/034)
- Preece, R. D., Briggs, M. S., Mallozzi, R. S., et al. 1998, *ApJL*, 506, L23, doi: [10.1086/311644](https://doi.org/10.1086/311644)
- Rees, M. J., & Mészáros, P. 2005, *ApJ*, 628, 847, doi: [10.1086/430818](https://doi.org/10.1086/430818)
- Rossi, E. M., Beloborodov, A. M., & Rees, M. J. 2006, *MNRAS*, 369, 1797, doi: [10.1111/j.1365-2966.2006.10417.x](https://doi.org/10.1111/j.1365-2966.2006.10417.x)
- Senno, N., Murase, K., & Mészáros, P. 2016, *PhRvD*, 93, 083003, doi: [10.1103/PhysRevD.93.083003](https://doi.org/10.1103/PhysRevD.93.083003)
- Svinkin, D., Frederiks, D., Ulanov, M., et al. 2023, *GRB Coordinates Network*, 33427, 1
- Vietri, M. 1995, *ApJ*, 453, 883, doi: [10.1086/176448](https://doi.org/10.1086/176448)
- Vurm, I., Beloborodov, A. M., & Poutanen, J. 2011a, *ApJ*, 738, 77, doi: [10.1088/0004-637X/738/1/77](https://doi.org/10.1088/0004-637X/738/1/77)
- . 2011b, *ApJ*, 738, 77, doi: [10.1088/0004-637X/738/1/77](https://doi.org/10.1088/0004-637X/738/1/77)
- Wang, X.-Y., & Dai, Z.-G. 2009, *ApJL*, 691, L67, doi: [10.1088/0004-637X/691/2/L67](https://doi.org/10.1088/0004-637X/691/2/L67)
- Waxman, E. 1995, *PhRvL*, 75, 386, doi: [10.1103/PhysRevLett.75.386](https://doi.org/10.1103/PhysRevLett.75.386)
- Waxman, E., & Bahcall, J. 1997, *PhRvL*, 78, 2292, doi: [10.1103/PhysRevLett.78.2292](https://doi.org/10.1103/PhysRevLett.78.2292)

Xiong, S., Wang, C., Huang, Y., & Gecam Team. 2023,
GRB Coordinates Network, 33406, 1

Yang, J., Ai, S., Zhang, B.-B., et al. 2022, Nature, 612, 232,
doi: [10.1038/s41586-022-05403-8](https://doi.org/10.1038/s41586-022-05403-8)

Yang, J., Zhao, X.-H., Yan, Z., et al. 2023, ApJL, 947, L11,
doi: [10.3847/2041-8213/acc84b](https://doi.org/10.3847/2041-8213/acc84b)

Zhang, B., & Kumar, P. 2013, PhRvL, 110, 121101,

doi: [10.1103/PhysRevLett.110.121101](https://doi.org/10.1103/PhysRevLett.110.121101)